Experimental and numerical Lattice-Boltzmann investigation of the Darrieus–Landau instability

Muhammad Tayyab[a], Basile Radisson[b,c], Christophe Almarcha[b], Bruno Denet[b], Pierre Boivin[a,*]

[a] *Aix Marseille Univ, CNRS, Centrale Marseille, M2P2, Marseille, France*
[b] *Aix Marseille Univ, CNRS, Centrale Marseille, IRPHE, Marseille, France*
[c] *Department of Aerospace and Mechanical Engineering, University of Southern California, Los Angeles, CA 90089-1191, USA*

ARTICLE INFO

ABSTRACT

We present an experimental and numerical investigation of the Darrieus–Landau instability in a quasi two-dimensional Hele-Shaw cell. Experiments and Lattice-Boltzmann numerical simulations are compared with Darrieus–Landau analytical theory, showing an excellent agreement for the exponential growth rate of the instability in the linear regime. The negative growth rate – second solution of the dispersion relation – was also measured numerically for the first time to the authors' knowledge. Experiments and numerical simulations were then carried out beyond the cutoff wavelength, providing good agreement even in the unexplored regime where Darrieus–Landau is supplanted by diffusive stabilization. Lastly, the non-linear evolution involving the merging of crests on the experimental flame front is also successfully recovered using both the Michelson–Sivashinsky equation integration and the Lattice-Boltzmann simulation.

1. Introduction

Lattice-Boltzmann (LB) methods have been proven very efficient in the field of low-Mach external aerodynamics and aeroacoustics [1,2]. However, although the first attempt of using LB methods for low Mach number combustion has been published twenty years ago [3], a lot of interest in LB methods for reactive flows has been observed only recently [4–6]. We proposed in [6,7] a hybrid LB framework (Lattice-Boltzmann/finite differences) able to study combustion for low-Mach flows. Among the tests in [6] was a preliminary study of the Darrieus–Landau instability of premixed flames, a very challenging test case for LB methods since it couples temperature and species fields to the velocity field. The underlying coupling between the Lattice-Boltzmann and finite differences solvers was further improved in [8], significantly improving the method stability.

Other numerical methods have been able to compute an important characteristic of the Darrieus–Landau instability, the growth rate of small amplitude perturbations as a function of wavenumber, for one-step chemistry [9,10] or for hydrogen–air flames [11], but it will be the first time that a LB method is able to describe this phenomenon. The comparison will not be limited to linear properties of the instability, but we will also show that the LB method also describes correctly the non linear evolution of the flame.

In this paper, we compare two-dimensional simulations with our hybrid LB method to quasi-2D experiments performed in a Hele-Shaw burner. Compared to [6] we will be able to obtain the full dispersion relation giving the growth rate as a function of wavenumber: it will be shown that this dispersion relation has the same form as that obtained in experiments, even beyond the cutoff wave number. Furthermore, we extend the comparison up to times where non-linearities play a significant role in the flame dynamics thereby demonstrating the ability of the method to correctly predict these complex phenomena.

2. Numerical set-up

The numerical simulations are carried out with the PROLB software using a pressure-based hybrid regularized thermal Lattice Boltzmann (LB) model coupled with a Finite Differences (FD) solver. The probability density function f_i (of finding gas particles at x with velocity c_i) is solved using hybrid regularized collision model [6]. The streaming and collision process can be expressed under discrete form as

$$f_i(t + \delta t, \boldsymbol{x}) = f_i^{\text{col}}(t, \boldsymbol{x} - \boldsymbol{c_i}\delta t),$$

$$f_i^{\text{col}}(t, \boldsymbol{x}) = f_i^{\text{eq}} + \left(1 - \frac{\delta t}{\bar{\tau}}\right)f_i^{\text{neq}} + \frac{\delta t}{2}F_i^E \qquad (1)$$

where $\bar{\tau}$ is a non-dimensional relaxation time, δt is the time-step, $\boldsymbol{c}_i$ is the ith discrete velocity of the D3Q19 lattice set, and f_i^{eq} and f_i^{neq} the equilibrium and non-equilibrium segments of the distribution function and F_i^E is the forcing term required to correctly recover the stress tensor [6,12]. Full expressions for f_i^{eq}, f_i^{neq}, F_i^E and their relation with the macroscopic variables are provided in Appendix A. Note that the expressions correspond to those presented in [6], with the addition of the recent developments presented in [8].

It can be shown via the Chapman–Enskog expansion [6,8] that the above system of equations is equivalent to solving the mass and momentum conservation equations

$$\frac{\partial \rho}{\partial t} + \frac{\partial}{\partial x_\alpha}(\rho u_\alpha) = 0,$$

$$\frac{\partial \rho u_\alpha}{\partial t} + \frac{\partial}{\partial x_\beta}(\rho u_\alpha u_\beta) = -\frac{\partial p}{\partial x_\alpha} + \frac{\partial \mathcal{T}_{\alpha\beta}}{\partial x_\beta} \qquad (2)$$

at second-order in time and space, where notations follow [13].

The FD solver consists of mass conservation of species k and enthalpy conservation equations solved through classical central difference approach. Temporal integration of the FD equations is explicit first-order in time, but the global order of the method is close to second-order [6,8,12]. Further details on the coupling between the two solvers are available in our recent publications [6–8,12]. The species conservation equation reads

$$\rho\frac{\partial Y_k}{\partial t} + \rho u_\alpha \frac{\partial Y_k}{\partial x_\alpha} = \frac{\partial}{\partial x_\alpha}(-\rho Y_k V_{k,\alpha}) + \dot{\omega}_k \qquad (3)$$

where $\dot{\omega}_k$ is the net chemical production rate of species k, and $V_{k,\alpha}$ is its diffusion velocity [13]. The energy conservation can be expressed in different ways, in this work we decide to consider the enthalpy conservation of a gas mixture with multi-component ideal gas thermodynamic closure:

$$h = \sum_{k=1}^{N} h_k Y_k \quad h_k = \int_{T_0}^{T} C_{p,k}(T)dT + \Delta h_{f,k}^0, \qquad (4)$$

where T and h are linked through NASA polynomials leading to the following enthalpy equation

$$\rho\frac{\partial h}{\partial t} + \rho u_\alpha \frac{\partial h}{\partial x_\alpha} = \frac{Dp}{Dt} - \frac{\partial q_\alpha}{\partial x_\alpha}. \qquad (5)$$

where $\frac{Dp}{Dt} = \frac{\partial p}{\partial t} + u_\alpha \frac{\partial p}{\partial x_\alpha}$ is neglected. The heat flux q_α reads

$$q_\alpha = -\lambda\frac{\partial T}{\partial x_\alpha} + \rho\sum_{k=1}^{N} h_k Y_k V_{k,\alpha}, \qquad (6)$$

with λ the thermal conductivity. Diffusion velocities are defined as in [6], using constant Schmidt number for each species (See Table B.1), and a correction velocity to ensure mass conservation [13].

3. Experimental set-up

The experiments are carried out in a Hele-Shaw burner [14–20]. The apparatus used here is made of two borosilicate glass plates (1500 × 500 × 5 mm) vertically oriented and separated by a $\Delta = 5$ mm gap, shown in Fig. 1. The burner is opened at the top, and closed at the bottom and on the two vertical sides. At the bottom of the facility a flow line controlled by two Bronkhorst EL-Flow series mass-flow regulators allows to fill the burner with a propane–air mixture with desired equivalence ratio φ. For all
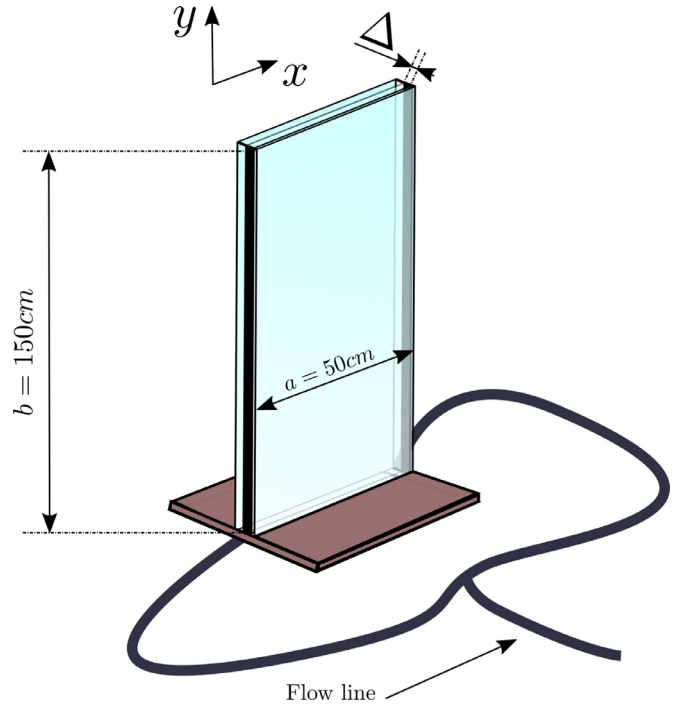

Fig. 1. Experimental set-up.

the experiments presented hereafter, the Hele-shaw burner is filled with a propane–air mixture $\varphi = 0.8$ with a flow rate such that the mixture velocity at the top of the burner is in excess to the flame speed, allowing the flame to remain anchored as a Bunsen flame at the top of the two glass plates. Then the mixture flow is stopped (in a repeatable manner thanks to a solenoid valve) and the flame starts its downwards propagation. The initial flat front is rapidly destabilized due to Darrieus–Landau effect. Initial perturbations are either magnified or damped according to their respective growth rate, leading to typical Darrieus–Landau wrinkled flame fronts. In order to measure the growth rate associated with perturbation of different wavelengths we make use of a forcing method to select the desired wavelength. For this purpose, a steel plate, laser-cut with a sinusoidal profile, is positioned at top of the burner next to the anchored flame (see [21] for details about the experimental technique). This technique allows to print an initial perturbation on the flame front. The flame front dynamics is then recorded using a high speed camera (Photron FASTCAM Mini AX200) and analyzed using an image processing python code (based on the scikit-image opensource library [22]).

4. Comparison and validation

4.1. Numerical setup

The equations solved with the Lattice-Boltzmann method correspond to two dimensional flames interacting with the velocity field and will be compared to quasi-2D experiments in the Hele-Shaw burner. However these equations do not correspond to the narrow-channel approximation [16] as the 5 mm gap used in the experiments is not sufficiently small.

Propane–air thermochemical properties are as follow:

- NASA polynomial coefficients for the thermodynamic closure $(p, T) = f(\rho, h)$ required in closing the governing equations (2), (3) and (5),
- Power-law for the viscosity, yielding transport properties via constant Prandtl and component-specific Schmidt numbers,

• One-step chemistry, where the pre-exponential parameter was chosen so the flame velocity and thickness would be in agreement with the dispersion relation. In particular, this leads to a laminar flame velocity lower than usual, to account for heat losses.

A detailed account on these thermo-chemical parameters is available in Appendix B.

In the following, we consider a two-dimensional rectangular computational domain uniformly discretized with $\delta_x = 10^{-4}$ m. The domain width corresponds exactly to one wave length $\frac{2\pi}{k}$ for the Linear regime analysis (Section 4.2). In the non-linear regime study Section 4.3 the domain width is 160 mm, corresponding to one third of the size of the Hele-Shaw cell represented in Fig. 1: in the experiment, the same initial profile is reproduced three times in the span-wise direction to improve periodicity. The time-step is maintained at $\delta_t = 7.217 \times 10^{-8}$ s, corresponding to an acoustic CFL of 0.63.

The right and left boundaries conditions are periodic, while a fixed wall is set at the bottom, and an open boundary conditions is considered at the top, letting the burnt gases escape.

The domain is initialized by computing first the one-dimensional premixed flame structure, e.g. $T_{1D}(y)$ for the temperature. That profile is then extended to the two-dimensional domain as $T(x, y, t = 0) = T_{1D}(y - f(x))$, where $f(x)$ is the desired geometrical perturbation:

• a single sine wave for the linear regime analysis (Section 4.2)
• a periodic experimental solution for the non-linear dynamics analysis (Section 4.3)

Buoyancy forces are not taken into account in the Lattice Boltzmann numerical scheme. For downward propagating flames such as those observed experimentally in the Hele-Shaw cell, the gravity term leads to slightly lower growth rates, and does not have a large influence on the non linear evolution for short times. Interesting papers on the role of gravity on the dispersion relation are [23] for two-dimensional flames and [24] in the narrow-channel approximation.

4.2. Linear regime analysis

The linear dynamics is analyzed by perturbing the flame front using sinusoidal waves. Initially, the amplitude of the waves are small and are expected to grow because of the Darrieus–Landau instability.

Considering that the thermal diffusive properties of the mixture depends on the temperature as $\rho D_{th} \propto T^\beta$ (with $\beta = 0.69$), the theoretical dispersion relation is then given by Clavin and Garcia [23] (see also [25]) :

$$A(k)\sigma^2 + B(k)\sigma + C(k) = 0, \tag{7}$$

where σ is the growth rate of the perturbation with wavenumber k. $A(k)$, $B(k)$, $C(k)$ are coefficients depending on gas expansion $E = \rho_u/\rho_b$, Markstein number $\mathcal{M}$, laminar flame speed u_L, flame thickness $d = D_{th}/u_L$, and Prandtl number Pr as

$$A(k) = \frac{E+1}{E} + \frac{E-1}{E} kd\left(\mathcal{M} - J\frac{E}{E-1}\right),$$

$$B(k) = u_L k\left(2 + 2Ekd(\mathcal{M} - J)\right), \tag{8}$$

$$C(k) = u_L^2 k^2\left((E-1)\frac{k}{k_c} - (E-1)\right),$$

where the cutoff wavenumber k_c verifies $k_c^{-1} = d(E^\beta + \frac{3E-1}{E-1}\mathcal{M} - \frac{2E}{E-1}J + (2Pr - 1)H)$. The integrals J and H can be found in [23,25]. The positive root σ_+ (the positive growth rate, leading to an

exponential amplification of the perturbations) of the quadratic Eq. (7) verifies approximately

$$\sigma_+ = ak - bk^2 + \mathcal{O}(k^3). \tag{9}$$

A straightforward development (see [17]) leads to

$$a = \frac{E}{E+1}\left[S - 1\right]u_L, \tag{10}$$

where $S = \sqrt{1 + E - \frac{1}{E}}$, the relation $\sigma = ak$ is the known Darrieus–Landau result without Markstein number effect, and

$$b = -du_L\left[\left(-a^2\frac{E-1}{E} - 2aE\right)\mathcal{M} + J(a^2 + 2aE) - \frac{E-1}{k_c d}\right]\bigg/2S. \tag{11}$$

This dispersion relation has also been obtained by Matalon and coworkers for temperature dependent diffusivities (see [26,27]).

It has been possible to measure experimentally the dispersion relation corresponding to Eq. (9) for 2D Bunsen flames [25] and recently some of the authors have measured the dispersion relation in a Hele-Shaw cell [17,21]. Numerically some measurements of growth rates have been performed, first for one-step chemistry [9,10,28] and recently for hydrogen–air flames [11,27,29].

Note that a negative root σ_- of the quadratic Eq. (7) also exists, we will show later that we are able to measure this negative growth rate in the numerical simulations. Anyway, as the precision in the calculation decreases when the damping increases, we will refer to the approximate formula, only valid for low wavenumbers:

$$\sigma_- = \frac{E}{E+1}[-S - 1]u_L k + \mathcal{O}(k^2). \tag{12}$$

This mode attenuates fast and the positive mode associated to σ_+ becomes dominant. This phenomenon is observed in the simulation results and is presented in Fig. 2. The initial instances of the growth are exponential and are defined in terms of both modes as:

$$A = A_0 e^{\sigma_+ t} + A_1 e^{\sigma_- t}, \tag{13}$$

where σ_+ and σ_- correspond to the growth rates of the positive and negative mode respectively.

Our initial condition is a front slightly harmonically perturbed compared to the plane front, imposed following the strategy presented in Section 4.1. Let us note however that the velocity field could not be chosen in order to only have the growing mode of the instability, so that we have a transient. However, the precise transient does not change our estimate for the negative growth rate.

The Amplitude (A), computed using Fourier Transform, is reported in Fig. 2, for an initial sinusoidal perturbation at $k = 0.52$ mm^{-1}. The fit of the positive mode (σ_+), $A = A_0 e^{\sigma_+ t}$ from Eq. (13) is represented in Fig. 2a. Furthermore, the initial presence of two modes is underlined in Fig. 2b, along with the fit of the negative mode (σ_-). We clearly see that fitting the solution as the linear combination mentioned in Eq. (13) is accurate for all times, provided the linear regime is valid, until the amplitude of the mode saturates due to nonlinear effect.

As seen from Eq. (9), the positive mode of the growth is of the form $\sigma \propto |k| - k^2$. The initial growth is measured and compared to the theoretical dispersion relation, written in the following way

$$\sigma = \frac{4\sigma_M}{k_c}\left(|k| - \frac{k^2}{k_c}\right), \tag{14}$$

where σ_M is the growth rate of the most amplified wavelength and k_c the cutoff wavenumber. This dispersion relation is then fitted on the computed results. In order to have a quantitative agreement with the experimental results (we will only show propane–air
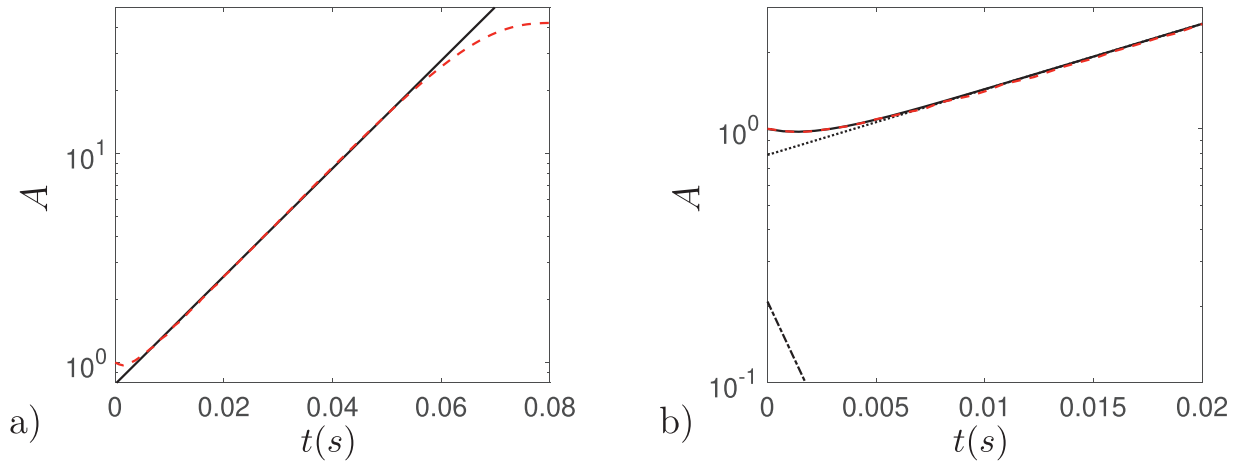
Fig. 2. Linear stage dynamics. (a) Evolution of normalized amplitude (A) calculated from numerical simulation (red dashed line) and gradient fit related to σ_+ (black solid line) presented over time where development of non-linear stage is observed. (b) Gradient fit related to σ_- (black dash–dotted line), gradient fit related to σ_+ (black dotted line), evolution of A (red dashed line) and sum of both fits related to σ_- and σ_+ (black solid line, indistinguishable from the red dashed line) presented at the initial instances where both modes (σ_+, σ_-) are present. (For interpretation of the references to color in this figure legend, the reader is referred to the web version of this article.)
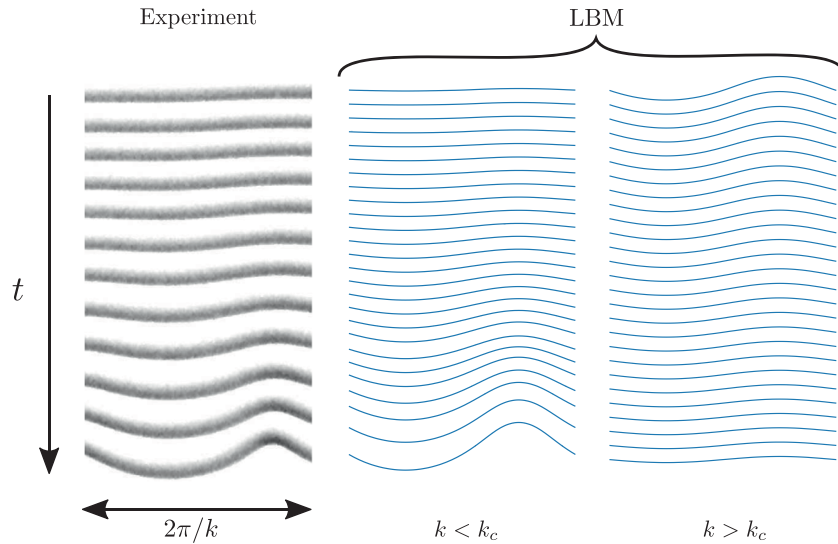

Fig. 3. Observation of growth and decay with wavenumbers higher and lower than k_c. Propagation of the flame is from top to bottom. Left: Growth at wavenumber lower than k_c. Right: Decay with wavenumber higher than k_c. Experimental (Black), and Numerical (blue) results. (For interpretation of the references to color in this figure legend, the reader is referred to the web version of this article.)
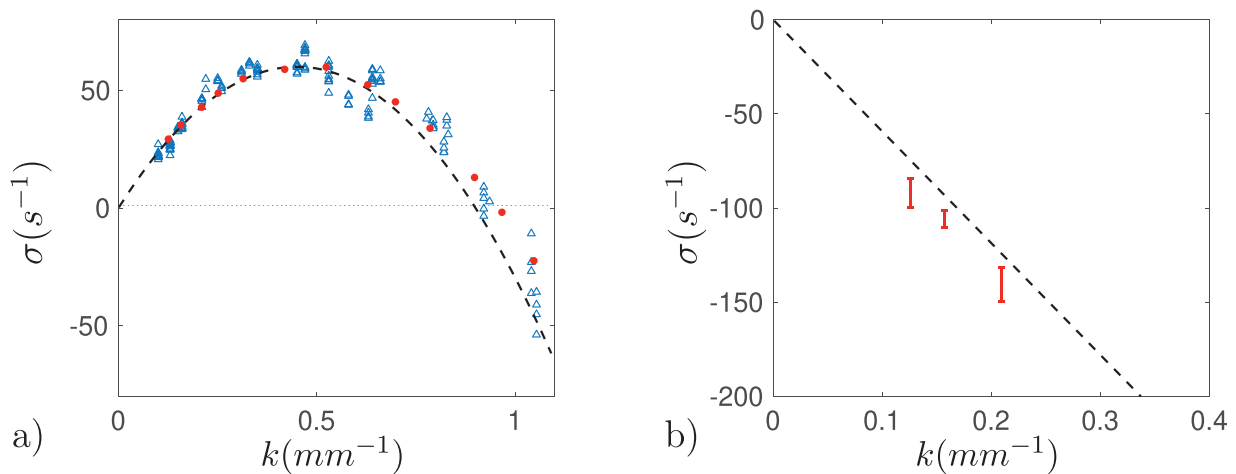

Fig. 4. Quantification and comparison of σ_+ and σ_-. (a) Growth rate (σ_+) measurement obtained from the experimental (blue triangles) and numerical (red circles) investigations. The theoretical dispersion relation (black dashed line) is then fitted with $\sigma_m = 60 s^{-1}$ and $k_c = 0.9\,mm^{-1}$. (b) Growth rates (σ_-) computed from simulations (red error bars) and theoretical solution from Eq. (12) (black dashed line). (For interpretation of the references to color in this figure legend, the reader is referred to the web version of this article.)
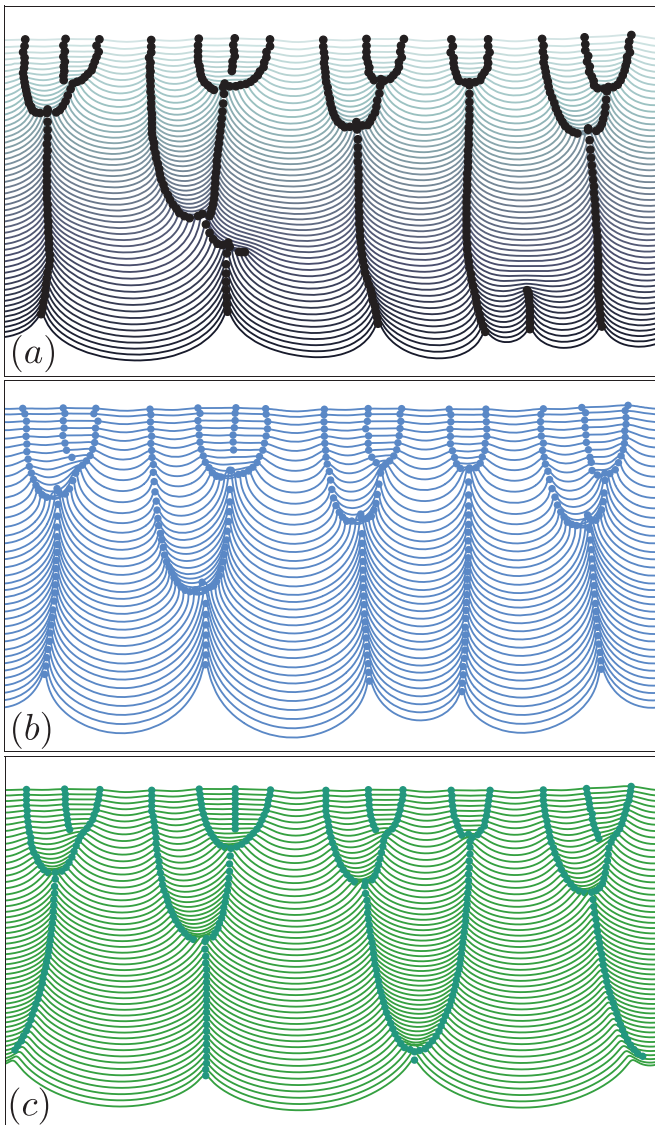
Fig. 5. Darrieus–Landau non linear evolution: (a) Experimental, (b) Numerical results and (c) MS equation starting from the same initial condition extracted from the experiment.

flames with equivalence ratio $\varphi = 0.8$), we choose in the numerical simulations the following parameters: $u_L = 0.177$ m/s, $E = 7.12$, $d = 0.53$ mm. Indeed the heat losses in the Hele-Shaw burner are large and lead to a weaker hydrodynamic instability than what is observed in a tube. u_L and d have been chosen to have an agreement with the experimental dispersion relation, in particular we have taken a value for u_L lower than the laminar flame speed for equivalence ratio $\varphi = 0.8$. Further details are given in Appendix B.

Figure 3 qualitatively shows the growth of perturbations at low wavenumber and decay for a wavenumber larger than k_c. The figure in black corresponds to an experiment (propane, $\varphi = 0.8$), and is compared to a numerical simulation for an unstable wavenumber. The figure on the right is a numerical simulation for a stable wavenumber (larger than k_c)

Quantitative agreement between numerical and experimental results is shown in Fig. 4a, where the numerical results (red circles) are compared to experiments (blue triangles) and to a fit of the dispersion relation (Eq. (14)). Note that we have also been able to measure the negative growth rate (Fig. 4b), which is compared to Eq. (12). The negative growth rates are presented as error

bars, given the difficulty of measuring accurately the quantity due to initial pressure perturbations present in the computational domain. Although the Lattice-Boltzmann measurements are slightly below the theoretical curve, the agreement is relatively good. To the knowledge of the authors, this is the first time in the literature that this negative growth rate is measured.

We thus have evidenced that our hybrid LBM method is able to correctly describe the linear premixed flame dynamics. It will be demonstrated in the next subsection that an agreement is also possible for the non linear evolution of the flame.

4.3. Non-linear dynamics

A very unstable premixed flame (a flame in a large domain, often called a self-turbulent flame [30]) leads to a complex non linear evolution involving merging and creation of new crests on the flame front. We have to show that our numerical simulations are able to describe correctly these effects. The LB simulations will thus be compared to experiments (see also [31]) and to the results of the Sivashinsky equation (or Michelson Sivashinsky: MS equation) [32]. This equation, solved with periodic boundary conditions, includes the linear dispersion relation (Eq. (14)), and a quadratic non-linearity and writes as:

$$\phi_t + \frac{u_A}{2}\phi_x^2 = \frac{4\sigma_M}{k_c}\left(\frac{\phi_{xx}}{k_c} + I(\phi, x)\right), \tag{15}$$

where ϕ stands for the vertical position of the front, x is the transverse coordinate and t the time. σ_M and k_c are the parameters given in Eq. (14), k_c is the cut-off wavenumber, $I(\phi, x)$ is the Landau operator corresponding to a multiplication by $|k|$ in Fourier space. The curvature term ϕ_{xx} comes from the thermal diffusive restabilization and is responsible for the damping of disturbances at small scales. Finally, ϕ_x^2 is a non linear term responsible for the formation of cusps. For low expansion E, u_A is close to the laminar flame speed, this is no longer the case for large E [33,34]. This parameter u_A is fitted to obtain amplitudes of the flame comparable to experiments.

In order, to compare the evolution given by the LBM integration and the MS model with an experiment, a flame is ignited at the top of the Hele-Shaw as a forced inverted V-flame. After a few instants of propagation, when the cusps start to be visible on the flame front, we extract the flame contour ($y = f(x)$) from the recorded images using an image processing algorithm. The obtained flame contour is then used as an initial condition for numerical integration (MS : $\phi(x, t = 0) = f(x)$ LBM : $T(x, y, t = 0) = T_{1D}(y - f(x))$).

In Fig. 5, we show the comparison between the evolution of experimental propane–air fronts ($\varphi = 0.8$), (Top figure, in black), the LB simulations, in blue, and the MS equation (Bottom figure, green lines). In each case, the positions of the cusps are highlighted, in order to better compare the three different evolutions.

As can be seen in the figure, the crest merging process is correctly described for short times by both the LB simulations and the Sivashinsky equation. The LB simulations are actually closer to experiments, which may be caused by the fact that the LB dispersion relation is slightly larger compared to the MS one close to k_c (see Fig. 4) or by the fact that flow non-linearities (neglected at the first order in gas expansion in the MS model) play a significant role. A difference between the experiments and the other figures is the creation of new cusps. This effect, which is not observed in the LB or MS simulations, could be caused by effects that we have neglected, such as additional noise, or gravity (the experimental premixed flames are actually propagating downwards).

5. Conclusion

Simulations performed with an hybrid Lattice-Boltzmann model for low-Mach reactive flows were presented in this paper for premixed flames unstable relative to the Darrieus–Landau instability. We were able to compare quantitatively the numerical results with quasi 2D experiments in a Hele-Shaw cell. The growth rates of the instability were measured by studying the development of small amplitude perturbations, and it was even possible to measure the decaying mode of the instability, showing the precision of the method. A correct agreement with experiments was also observed for the non linear evolution of the flame front.

Declaration of Competing Interest

The authors whose names are listed immediately below certify that they have NO affiliations with or involvement in any organization or entity with any financial interest (such as honoraria; educational grants; participation in speakers bureaus; membership, employment, consultancies, stock ownership, or other equity interest; and expert testimony or patent-licensing arrangements), or non-financial interest (such as personal or professional relationships, affiliations, knowledge or beliefs) in the subject matter or materials discussed in this manuscript.

Acknowledgements

Appendix A. Expressions for the LBM solver

In the low-Mach number approximation, the equilibrium function can be truncated at second-order as

$$f_i^{eq} = w_i \left[\rho\theta + \frac{\rho c_{i\alpha} u_\alpha}{c_s^2} + \frac{\mathcal{H}_{i,\alpha\beta}^{(2)} a_{\alpha\beta}^{(2),eq}}{2c_s^4} \right],$$

$$f_i^{neq} = \frac{\omega_i}{2c_s^4} \mathcal{H}_{i,\alpha\beta}^{(2)} a_{\alpha\beta}^{neq}, \tag{A.1}$$

where,

$$\mathcal{H}_{i,\alpha\beta}^{(2)} = c_{i\alpha} c_{i\beta} - c_s^2 \delta_{\alpha\beta}, \quad a_{\alpha\beta}^{(2),eq} = \rho u_\alpha u_\beta,$$

$$a_{\alpha\beta}^{neq} = \mathcal{H}_{i,\alpha\beta}^{(2)} \left(f_i - f_i^{eq} \right), \tag{A.2}$$

θ is the normalized temperature linked with pressure as $p = \rho c_s^2 \theta$, using ideal gas law, w_i is the weight coefficient related to the discrete velocity $\boldsymbol{c}_i$ and c_s is the lattice sound speed. Note that the equilibrium function differs from [6], and was adapted from [8], enhancing numerical stability. In particular, the pressure contribution θ is now inserted in the zeroth moment of (A.2) rather than higher moments as in [6].

Consequently [8], the reconstruction of macroscopic variables now read

$$\rho(t + \delta t, \boldsymbol{x}) = \sum f_i^{col} + \rho(t, \boldsymbol{x})(1 - \theta(t, \boldsymbol{x}))$$

$$(\rho u_\alpha)(t + \delta t, \boldsymbol{x}) = \sum c_{i\alpha} f_i^{col}. \tag{A.3}$$

Finally, the required forcing term is obtained as

$$F_i^E = \frac{\omega_i}{2c_s^4} \mathcal{H}_{i,\alpha\beta}^{(2)} \left[c_s^2 u_\alpha \rho_{,\beta} + c_s^2 u_\beta \rho_{,\alpha} + \delta_{\alpha\beta}\rho c_s^2 \left(\frac{2}{3} - \frac{\eta_B}{\mu}\right) u_{\gamma,\gamma} \right.$$

$$\left. + \Delta(\rho u_\alpha u_\beta) - \delta_{\alpha\beta} c_s^2 \Delta[\rho(1-\theta)] \right], \tag{A.4}$$

with η_B is the bulk viscosity, and

$$\Delta(\rho u_\alpha u_\beta) = (\rho u_\alpha u_\beta)(t + \delta t, \boldsymbol{x}) - (\rho u_\alpha u_\beta)(t, \boldsymbol{x}),$$
$$\Delta[\rho(1-\theta)] = \rho(t + \delta t, \boldsymbol{x})(1 - \theta(t + \delta t, \boldsymbol{x}))$$
$$- \rho(t, \boldsymbol{x})(1 - \theta(t, \boldsymbol{x})). \tag{A.5}$$

Appendix B. Numerical simulation parameters

In this article we consider one-step propane/air mixture with 5 species: C_3H_8, O_2, H_2O, CO_2, N_2. The thermal and species diffusion coefficients are calculated using Schmidt and Prandtl numbers, detailed in Table B.1. Along with the use of viscosity's power law,

$$\mu = \mu_0 \left(\frac{T}{T_0}\right)^\beta, \tag{B.1}$$

where reference viscosity $\mu_0 = 1.782 \times 10^{-5}$, reference Temperature $T_0 = 300$ K and coefficient $\beta = 0.69$. Furthermore, classical NASA polynomials for each species k are used to define the thermodynamic properties.

In order to define the chemical source term a one-step Arrhenius kinetic model is used, following global reaction $C_3H_8 + 5\ O_2 \longrightarrow 3\ CO_2 + 4\ H_2O$, associated with the kinetic rate $\omega = k_{chem}.C_{C_3H_8}.C_{O_2}.e^{-E_a/RT}$, where $k_{chem} = 8.77 \times 10^{13}$ cm^3 mol^{-1} s^{-1}, $E_a = 30$ kcal/mol, and C_i are the molar concentrations for species i. The initial conditions used in order to compute 1-D premixed profiles at equivalence ratio ($\phi = 0.8$) are detailed in Table B.2.

Given that the model presented in Section 2 does not account for heat losses, experimental results cannot be compared to the simulated result. In order to overcome this problem, we used Eq. (10) and relation $\sigma = ak$ to compute the flame speed $S_L^{exp} = 0.177$ m/s which corresponds to growth obtained experimentally at lower wave-numbers. Furthermore, the original value $k_{chem} = 9.9 \times 10^{13}$ cm^3 mol^{-1} s^{-1} [7] associated to the chemical reaction rate is modified to $k_{chem} = 8.77 \times 10^{13}$ cm^3 mol^{-1} s^{-1} in order to recover S_L^{exp} in our simulations. Lastly, to assure that we recover comparable σ_m, flame thickening model [35] with a factor of 1.48 is used to recover the flame thickness. These adjustments allow us to compare the growth rates with the experimental results.

Table B1
Prandtl number and Schmidt numbers for each specie.

Pr	0.682
$S_{C_3H_8}$	1.241
S_{O_2}	0.728
S_{CO_2}	0.941
S_{H_2O}	0.537
S_{N_2}	0.690

Table B2
Initial conditions: 1-D domain is initialized with fresh gases corresponding to (0: L/2) and burnt gases (L/2: L).

Variables	Fresh gases	Burnt gases
T	300 K	2069.98 K
p	1 atm	1 atm
$Y_{C_3H_8}$	4.88×10^{-2}	6.76×10^{-15}
Y_{O_2}	2.21×10^{-1}	4.39×10^{-2}
Y_{CO_2}	9.74×10^{-18}	1.46×10^{-1}
Y_{H_2O}	1.54×10^{-13}	8.02×10^{-2}
Y_{N_2}	7.29×10^{-1}	7.29×10^{-1}

References

[1] S. Chen, G.D. Doolen, Lattice Boltzmann method for fluid flows, Annu. Rev. Fluid Mech. 30 (1) (1998) 329–364.

[2] A. Sengissen, J.-C. Giret, C. Coreixas, J.-F. Boussuge, Simulations of lagoon landing-gear noise using Lattice Boltzmann solver, 21st AIAA/CEAS Aeroacoustics Conference (2015), p. 2993.

[3] O. Filippova, D. Hänel, A novel lattice BGK approach for low mach number combustion, J. Comput. Phys. 158 (2) (2000) 139–160.

[4] C. Lin, K.H. Luo, Mesoscopic simulation of nonequilibrium detonation with discrete Boltzmann method, Combust. Flame 198 (2018) 356–362.

[5] S.A. Hosseini, H. Safari, N. Darabiha, D. Thévenin, M. Krafczyk, Hybrid Lattice Boltzmann-finite difference model for low mach number combustion simulation, Combust. Flame 209 (2019) 394–404.

[6] M. Tayyab, S. Zhao, Y. Feng, P. Boivin, Hybrid regularized Lattice-Boltzmann modelling of premixed and non-premixed combustion processes, Combust. Flame 211 (2020) 173–184.

[7] Y. Feng, M. Tayyab, P. Boivin, A Lattice-Boltzmann model for low-mach reactive flows, Combust. Flame 196 (2018) 249–254.

[8] G. Farag, S. Zhao, T. Coratger, P. Boivin, G. Chiavassa, P. Sagaut, A pressure-based Lattice-Boltzmann method for the simulation of compressible flows, Phys. Fluids (2020). accepted

[9] B. Denet, P. Haldenwang, A numerical study of premixed flames Darrieus-Landau instability, Combust. Sci. Technol. 104 (1–3) (1995) 143–167.

[10] S. Kadowaki, T. Hasegawa, Numerical simulation of dynamics of premixed flames: flame instability and vortex–flame interaction, Prog. Energy Combust. Sci. 31 (3) (2005) 193–241.

[11] C.E. Frouzakis, N. Fogla, A.G. Tomboulides, C. Altantzis, M. Matalon, Numerical study of unstable hydrogen/air flames: Shape and propagation speed, Proc. Combust. Inst. 35 (2015) 1087–1095.

[12] Y. Feng, P. Boivin, J. Jacob, P. Sagaut, Hybrid recursive regularized thermal lattice Boltzmann model for high subsonic compressible flows, J. Comput. Phys. 394 (2019) 82–99.

[13] T. Poinsot, D. Veynante, Theoretical and Numerical Combustion, RT Edwards, Inc., 2005.

[14] G. Joulin, G. Sivashinsky, Influence of momentum and heat losses on the large-scale stability of quasi-2D premixed flames, Combust. Sci. Technol. 98 (1–3) (1994) 11–23.

[15] J. Sharif, M. Abid, P.D. Ronney, Premixed-gas flame propagation in Hele-Shaw cells, 1st Joint U.S. Sections Combustion Institute Meeting, 1999. Washington, DC; United States

[16] D. Fernández-Galisteo, V.N. Kurdyumov, P.D. Ronney, Analysis of premixed flame propagation between two closely-spaced parallel plates, Combust. Flame 190 (2018) 133–145.

[17] E. Al Sarraf, C. Almarcha, J. Quinard, B. Radisson, B. Denet, P. Garcia-Ybarra, Darrieus-Landau instability and Markstein numbers of premixed flames in a Hele-Shaw cell, Proc. Combust. Inst. 37 (2) (2019) 1783–1789.

[18] H.J. Jang, G.M. Jang, N.I. Kim, Unsteady propagation of premixed methane/propane flames in a mesoscale disk burner of variable-gaps, Proc. Combust. Inst. 37 (2) (2019) 1861–1868.

[19] M.M. Alexeev, O.Y. Semenov, S.E. Yakush, Experimental study on cellular premixed propane flames in a narrow gap between parallel plates, Combust. Sci. Technol. (2018) 1–20.

[20] F. Veiga-López, D. Martínez-Ruiz, E. Fernández-Tarrazo, M. Sánchez-Sanz, Experimental analysis of oscillatory premixed flames in a Hele-Shaw cell propagating towards a closed end, Combust. Flame 201 (2019) 1–11.

[21] E. Al Sarraf, C. Almarcha, J. Quinard, B. Radisson, B. Denet, Quantitative analysis of flame instabilities in a Hele-Shaw burner, Flow Turbul. Combust. 101 (3) (2018) 851–868.

[22] S. van der Walt, J.L. Schönberger, J. Nunez-Iglesias, F. Boulogne, J.D. Warner, N. Yager, E. Gouillart, T. Yu, The scikit-image contributors, scikit-image: image processing in python, PeerJ 2 (2014) e453.

[23] P. Clavin, P. Garcia, The influence of the temperature dependence of diffusivities on the dynamics, J. Méc. Théor. Appl. 2 (2) (1983) 245–263.

[24] D. Fernández-Galisteo, V.N. Kurdyumov, Impact of the gravity field on stability of premixed flames propagating between two closely spaced parallel plates, Proc. Combust. Inst. 37 (2) (2019) 1937–1943.

[25] J.-M. Truffaut, G. Searby, Experimental study of the Darrieus-Landau instability on an inverted-V flame, and measurement of the Markstein number, Combust. Sci. Technol. 149 (1–6) (1999) 35–52.

[26] M. Matalon, C. Cui, J.K. Bechtold, Hydrodynamic theory of premixed flames: effects of stoichiometry, variable transport coefficients and arbitrary reaction orders, J. Fluid Mech. 487 (2003) 179–210.

[27] C. Altantzis, C.E. Frouzakis, A.G. Tomboulides, M. Matalon, K. Boulouchos, Hydrodynamic and thermodiffusive instability effects on the evolution of laminar planar lean premixed hydrogen flames, J. Fluid Mech. 700 (2012) 329–361.

[28] P.E. Lapenna, R. Lamioni, G. Troiani, F. Creta, Large scale effects in weakly turbulent premixed flames, Proc. Combust. Inst. 37 (2) (2019) 1945–1952.

[29] L. Berger, K. Kleinheinz, A. Attili, H. Pitsch, Characteristic patterns of thermodiffusively unstable premixed lean hydrogen flames, Proc. Combust. Inst. 37 (2) (2019) 1879–1886.

[30] C. Almarcha, J. Quinard, B. Denet, E. Al-Sarraf, E. Laugier, E. Villermaux, Experimental two dimensional cellular flames, Phys. Fluids 27 (2015) 091110.

[31] C. Almarcha, B. Radisson, E. Al Sarraf, E. Villermaux, B. Denet, J. Quinard, Interface dynamics, pole trajectories, and cell size statistics, Phys. Rev. E 98 (3) (2018) 030202.

[32] G. Sivashinsky, Nonlinear analysis of hydrodynamic instability in laminar flames—I. Derivation of basic equations, Acta Astronaut. 4 (1977) 1177–1206.

[33] G. Sivashinsky, P. Clavin, On the nonlinear theory of hydrodynamic instability in flames, J. Phys. 48 (2) (1987) 193–198.

[34] K.A. Kazakov, On-shell description of stationary flames, Phys. Fluids 17 (3) (2005) 032107.

[35] O. Colin, F. Ducros, D. Veynante, T. Poinsot, A thickened flame model for large eddy simulations of turbulent premixed combustion, Phys. Fluids 12 (2000) 1843.